Construction and Building Materials 339 (2022) 127689

Contents lists available at ScienceDirect

Construction and Building Materials

journal homepage: www.elsevier.com/locate/conbuildmat

Compactability and mechanical properties of cold recycled mixes prepared with different nominal maximum sizes of RAP

P. Orosa [a,b,*], G. Orozco [b], J.C. Carret [b], A. Carter [b], I. Pérez [a], A.R. Pasandín [a]

[a] Civil Engineering Department, E. T. S. de Ingeniería de Caminos, Canales y Puertos, Universidade da Coruña (UDC), A Coruña, Spain
[b] Construction Engineering Department, École de Technologie Supérieure (ÉTS), Montréal, Canada

ARTICLE INFO

Keywords:
Cold recycling
RAP
Gradation
Bitumen Emulsion
Gyratory compactor
Impact compactor
Indirect Tensile Strength (ITS)
Complex Modulus
Indirect Tensile Stiffness Modulus (ITSM)
Semi-Circular Bending test (SCB)

ABSTRACT

The use of cold recycled asphalt mixtures (CRM) has been soaring during recent years. Reclaimed Asphalt Pavement (RAP) is the main component of CRM, and despite the numerous studies on CRM, the impact of different RAP types has not been deeply studied. This study compares the volumetric and several mechanical properties of CRM prepared with RAP from two different sources and with various nominal maximum sizes (NMS). The mix design was fixed, and specimens were prepared using gyratory and impact compactors. Densities were measured before and after accelerated curing. Stiffness of CRM was investigated with Indirect Tensile Stiffness Modulus, tension–compression, and dynamic tests. Additionally, the cracking behavior was evaluated with Indirect Tensile Strength and Semi-Circular Bending tests. The particle size distribution was a key factor in the compactability of the CRMs studied. Together with temperature, the most influential factor on the studied mechanical properties was the air void content, while the differences in NMS showed no clear trends.

1. Introduction

Due to the economic and environmental situation experienced in recent years, there has been significant growth in the use of cold recycled mixtures (CRM) in the paving industry [1,2]. This kind of mixture allows the partial or total substitution of the natural aggregate used in traditional bituminous mixes, by recycled aggregate coming from the milling of worn-out roads, known as Reclaimed Asphalt Pavement (RAP). The possibility of production at room temperature is definitely one of the main benefits of this technique when compared with traditional hot mixes (HMA). This lower working temperature is achieved by using bitumen emulsion or foamed bitumen as the binder in the CRM, which presents lower viscosities than traditional bitumen, thereby allowing the mixing and compaction operations to be done at lower temperatures, with the consequent important environmental and economic advantages [1–7]. In this paper, only mixtures with bitumen emulsion were studied. A certain amount of water is also added to CRM, which helps to disperse the emulsion to have a better coating and provides additional workability and compactability [7]. It is precisely the presence of water in the early stages after manufacture, when CRMs show the lowest mechanical properties [8,9]. The time required for the CRMs to develop these characteristics is known as curing, and is one of their main drawbacks.

Considering the wide variety of RAP sources that can be found due to the different materials that are originally used on roads, the properties of CRM can vary between mixes. Classifications based on aggregate properties exist for virgin aggregates included in traditional mixes, but so far there is no such prescription for RAP [10–12]. In fact, several authors studied the differences observed in CRM properties when using RAP coming from different sources [13,14], as well as with different gradations [15,16]. Not only does the origin of the RAP vary, but also, depending on the degree of milling applied during the recycling process, the RAP nominal maximum grain size (NMS) and distribution also vary, resulting in different properties of the final cold recycled mixture obtained. Hence, this study is the result of work carried out at École de technologie supérieure (ÉTS) in Montreal (Canada) and at ETS de Ingeniería de Caminos, Canales y Puertos (ETSICCP) of the Universidade da Coruña (UDC) in Spain, showing the impact on the volumetric and mechanical properties of CRM prepared with RAP from different sources and with different particle sizes.

* Corresponding author.
E-mail addresses: p.orosa@udc.es (P. Orosa), gabriel.orozco.1@etsmtl.ca (G. Orozco), jean-claude.carret@etsmtl.ca (J.C. Carret), alan.carter@etsmtl.ca (A. Carter), iperez@udc.es (I. Pérez), arodriguezpa@udc.es (A.R. Pasandín).

https://doi.org/10.1016/j.conbuildmat.2022.127689
Received 18 March 2022; Received in revised form 26 April 2022; Accepted 26 April 2022
Available online 3 May 2022

2. Aim and scope

In this study, the influence of the source and nominal maximal size of RAP, and compaction method on the volumetric and mechanical properties of laboratory-prepared CRM was evaluated. For this purpose, a specific mix design was established in terms of dosing, mixing, and compaction parameters, and different mixes were prepared. At ÉTS, RAP from a single source was used and three mixtures were produced varying the NMS. The mixture prepared at UDC contains the same amount of emulsion and water, but was prepared with a different RAP source with a given NMS of 22.4 mm. For these four mixtures, prepared with both gyratory and Marshall compaction, the volumetric properties before and after curing were analyzed. In addition, two critical mechanical behaviors were evaluated: stiffness and mechanical failure behavior. At ÉTS, stiffness characterization was performed with the Indirect Tensile Stiffness Modulus (ITSM) test, as well as with the dynamic impact resonance (IR) test and the cyclic tension–compression (TC) test, to determine the Complex Modulus (CM). The feasibility of using the novel, non-destructive and fast dynamic IR test as a substitute of the traditional TC test was discussed. Additionally, mechanical failure behavior was investigated with the Indirect Tensile Strength (ITS) test and Semi–Circular Bending (SCB) test; while at UDC, the mechanical characterization only comprised ITS tests. The obtained mechanical properties were compared and analyzed as a function of RAP NMS, compaction procedure, air void content, and test temperature.

3. Materials

3.1. Mixtures composition

The solid phase of the mixes studied in the present work was entirely composed by RAP. The three grain sizes studied in ÉTS were produced by varying the NMS of a single RAP sourced from a quarry near Montreal (Quebec). The original 0/20 RAP source was sieved to obtain NMS of 5 mm, 10 mm, and 20 mm (Fig. 1). The characteristics of the RAP are shown in the Table 1.

The RAP used to prepare the mixtures studied at UDC (Spain) was obtained from a local quarry in the province of A Coruña (Galicia), and its properties are also shown in Table 1. All the particle size distributions are presented together in Fig. 2, and Fig. 1 allows visual comparison between them.

The bitumen emulsion used in this research work at ÉTS was a CSS-1 type (ASTM D2397), and the main properties of which along with the residual binder properties obtained after extraction are listed in Table 1. The bituminous emulsion used in the UDC was a C60B5 REC (EN 13808), and its properties are also summarized in Table 1. For all the mixes considered in this study, the binder content (BC) and the added water content (AWC) were fixed at 2.00% and 1.92%, respectively, by mass of dried RAP in all the mixes studied. The AWC is an extra water content, in addition to the water included in the emulsion. The binder and water contents were obtained at UDC as the optimum proportions according to the Spanish PG-4 [17]. These same proportions were used in previous research and were used here to facilitate comparison within mixes [8,16–19].

3.2. Mixing, compaction, and curing procedures

All specimens, both those manufactured at ÉTS and at UDC, were mechanically mixed following the same steps and timing as in previous research works on cold recycling mixtures [17,18,20]. In the first step, RAP and added water were incorporated and mixed together for 60 s. The corresponding emulsion content was then added and the mixing was

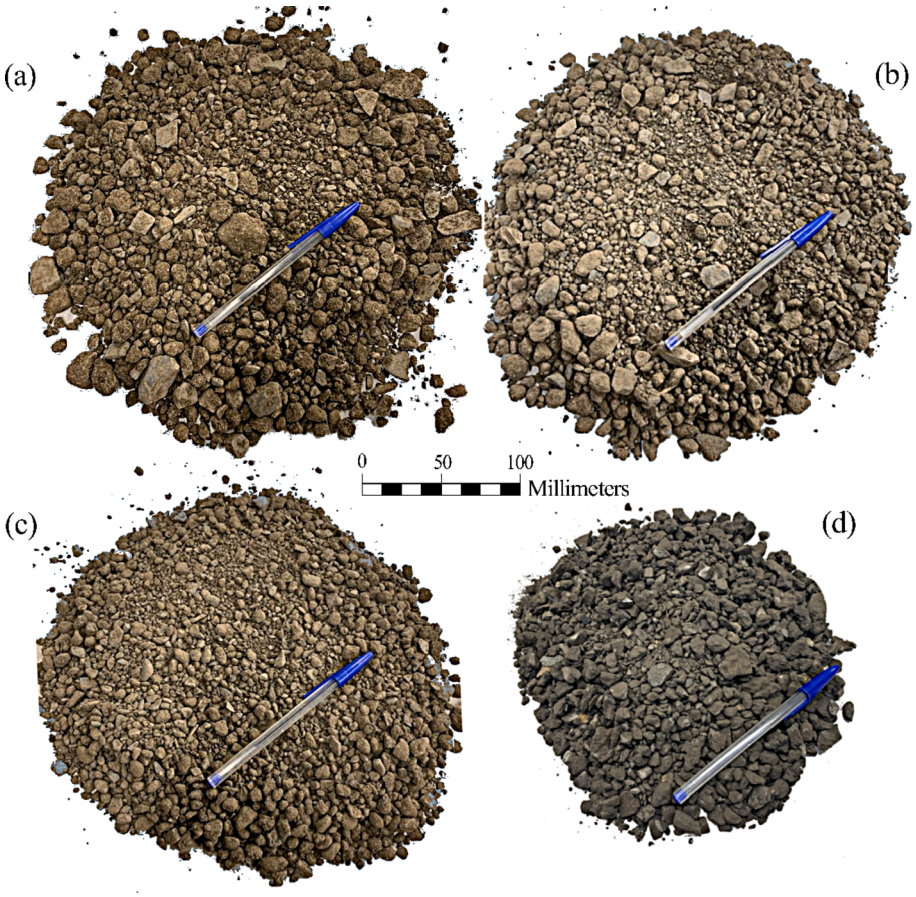

Fig. 1. Comparison of the different RAP employed: (a) ÉTS RAP 0/20, (b) ÉTS RAP 0/10, (c) ÉTS RAP 0/5, and (d) UDC RAP 0/22.

Table 1
RAP, bitumen emulsion, and residual binder properties.

ÉTS			
RAP properties	**Standard**	**Unit**	**Value**
Binder content	ASTM D6307	%	5.01
Nominal maximum particle dimension	ASTM D448–03	mm	20
Maximum specific gravity	ASTM C127–128	kg/m^3	2599
Emulsion and residual binder properties			
Residue content (bitumen)	ASTM D6997–12	%	62.8
Storage stability @ 24 h	ASTM D6930–10	%	0.10
Penetration @ 25 °C (bitumen)	ASTM D5–13	dmm	170
Saybolt Furol viscosity @ 25 °C	ASTM 7496	°C	28.1
UDC			
RAP properties	**Standard**	**Unit**	**Value**
Binder content	NLT–164/90	%	7.81
Nominal maximum particle dimension	EN 933–1	mm	22.4
Maximum specific gravity	EN 1097–6	kg/m^3	2560
Emulsion and residual binder properties			
Residue content (bitumen)	EN 1428	%	60
Penetration (bitumen)	EN 1427	dmm	170
Softening point	EN 1426	°C	36.50

continued for an additional 90 s, thereby ensuring the correct coating of the RAP, but preventing the breakage of the emulsion [20].

The compaction of the specimens was performed immediately once the mixing process was completed. Specimens in this study were compacted using the gyratory and impact procedures. The shear gyratory compaction (SGC) was carried out using 100 and 150 mm diameter molds, constant pressure of 600 kPa, and speed of 30 rpm, the internal angle used at ÉTS was 1.16°, while at UDC it was 0.82°, in accordance with each gyratory compactor specifications. A total of 100 and 200 gyrations were applied depending on the specimen group (Table 2). The impact compaction (Marshall) was also performed with 100 mm diameter molds, by applying 50 blows per face.

Gyratory-compacted specimens were stable enough to be demolded by extrusion after compaction. Impact-compacted specimens were demolded 24 h after compaction to prevent damage. All specimens, once demolded, were placed to cure in unsealed conditions in an oven at 50 °C for 72 h.

In order to differentiate the studied mixes, a specific nomenclature was used. Table 2 summarizes the different groups of specimens prepared, classifying them according to their source (ETS or UDC) and NMS (22.4, 20, 10, or 5 mm) of RAP, the type of compaction (G or M, for gyratory or Marshall compaction, respectively) and energy used (100 or 200 gyrations, or 50 blows), and the diameter (100 or 150 mm); also indicating the number of specimens, and the tests performed in each case.

4. Experimental program

The experimental program included an analysis of the volumetric properties and compaction of the different groups of specimens, and a subsequent extensive mechanical characterization. The study of mechanical behavior focused on two major aspects of bituminous materials: stiffness and cracking behavior. For the study of the mechanical behavior, the following tests were carried out: Indirect Tensile Stiffness Modulus (ITSM), Complex modulus (CM) using both dynamic impact resonance (IR) and cyclic tension–compression (TC) tests, Indirect Tensile Strength (ITS) and Semi-Circular Bending (SCB). Since the modulus tests were non-destructive, the same 100 mm–diameter specimens were used for ITSM and dynamic IR tests, and finally, they were subjected to ITS. To ensure the maintenance of the test temperatures, the tests were carried out inside climatic chambers at the corresponding temperature.

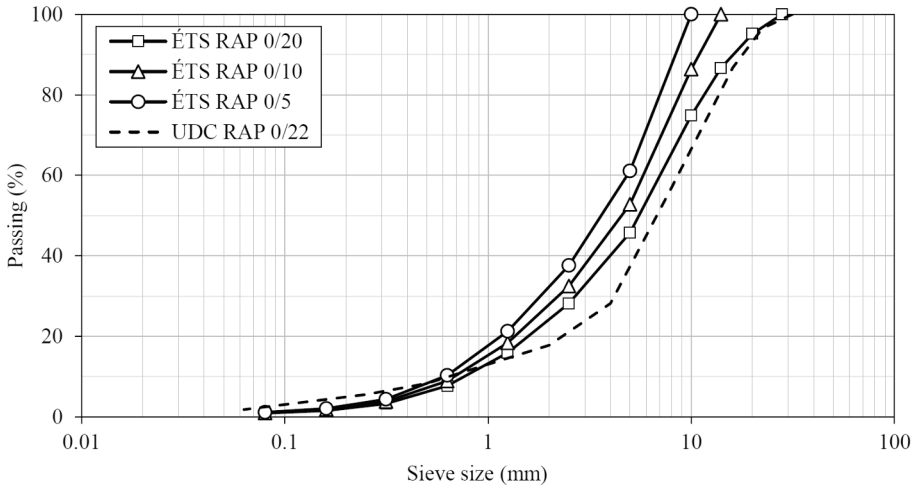

Fig. 2. RAP size distributions.

Table 2
Characteristics of the manufactured specimen.

ÉTS				
Specimen groups	**NMS**	**Compaction**	**N° of specimens**	**Tests**
ETS20_G100_D100	20 mm	SGC 100 gyrations	4	Volumetric
ETS10_G100_D100	10 mm	Ø* 100 mm	4	ITSM
ETS5_G100_D100	5 mm		4	IR
ETS20_M50_D100	20 mm	Marshall 50 blows	4	ITS
ETS10_M50_D100	10 mm	Ø 100 mm	4	
ETS5_M50_D100	5 mm		4	
ETS20_G200_D100	20 mm	SGC 200 gyrations	3	Volumetric
ETS10_G200_D100	10 mm	Ø 100 mm	3	ITS
ETS5_G200_D100	5 mm		3	
ETS20_G100_D150	20 mm	SGC 100 gyrations	1 (8 SCB)	Volumetric
ETS10_G100_D150	10 mm	Ø 150 mm	1 (8 SCB)	SCB
ETS5_G100_D150	5 mm		1 (8 SCB)	
UDC				
Specimen groups	**NMS**	**Compaction**	**N° of specimens**	**Tests**
UDC22_G100_D100	22.4 mm	SGC Ø 100 mm 100 gyr	4	Volumetric
UDC22_G200_D100		200 gyr	4	ITS
UDC22_M50_D100		Marshall 50 blows Ø 100 mm	4	

*Ø = diameter of the specimens.

4.1. Volumetric properties

The theoretical maximum specific gravity (ρ_m) of the four mixtures considered was calculated in accordance to the ASTM D2041 at ÉTS, and according to EN 12697–5 at UDC. Specimens compacted with gyratory and Marshall procedures were weighed and measured just after compaction, before curing, as well as after the curing process, thereby assessing the geometric bulk densities (ρ_b) and their equivalent air void contents (V_a) in each case (Eq. (1)), always under stable laboratory conditions. For the gyratory compacted specimens, the compaction rate of the different mixes was analyzed by comparing the compaction curves with 200 gyrations.

$$V_a(\%) = \frac{\rho_m - \rho_b}{\rho_m} \cdot 100 \quad (1)$$

4.2. Stiffness characterization

4.2.1. Indirect Tensile stiffness modulus (ITSM)

The ITSM test was performed in accordance with EN 12697–26 (Annex C). This test evaluates the stiffness modulus by means of a series of 10 vertical load pulse applications characterized by a rise time of 124 ± 4 ms. The tests were carried out in deformation control mode with a recurrence time of 3.0 s. The stiffness modulus was obtained for each pulse using Eq. (2):

$$ITSM = \frac{F \cdot (R + 0.27)}{L \cdot H} \quad (2)$$

Where F means the maximum value of the vertical repeated load applied, H means the horizontal strain amplitude (set at 7 ± 2 μm), L means the average thickness of the specimen and R means Poisson's ratio (assumed equal to 0.35).

The test was performed on 100 mm diameter specimens of the groups compacted with 100 gyrations of SGC and 50 Marshall blows (Table 2), thereby comparing the different NMS of RAP and both compaction methods. The ITSM value of each specimen was calculated as the average of the test performed along both diameters. Three different temperatures were used, –20, 0, and 20 °C, and the specimens were conditioned for 4 h.

4.2.2. Dynamic impact resonance (IR) test on disc-shaped specimen

For the dynamic IR tests, the 100 mm diameter specimens of each group previously used for the ITSM tests were reused. Following the

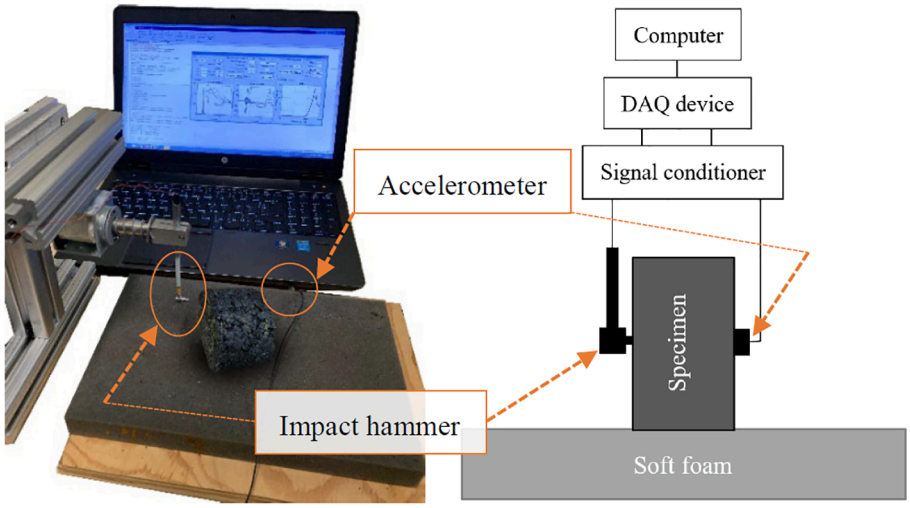

Fig. 3. Dynamic test set-up for the longitudinal mode of vibrations (example for specimen 4 of ETS20_G100_D100).

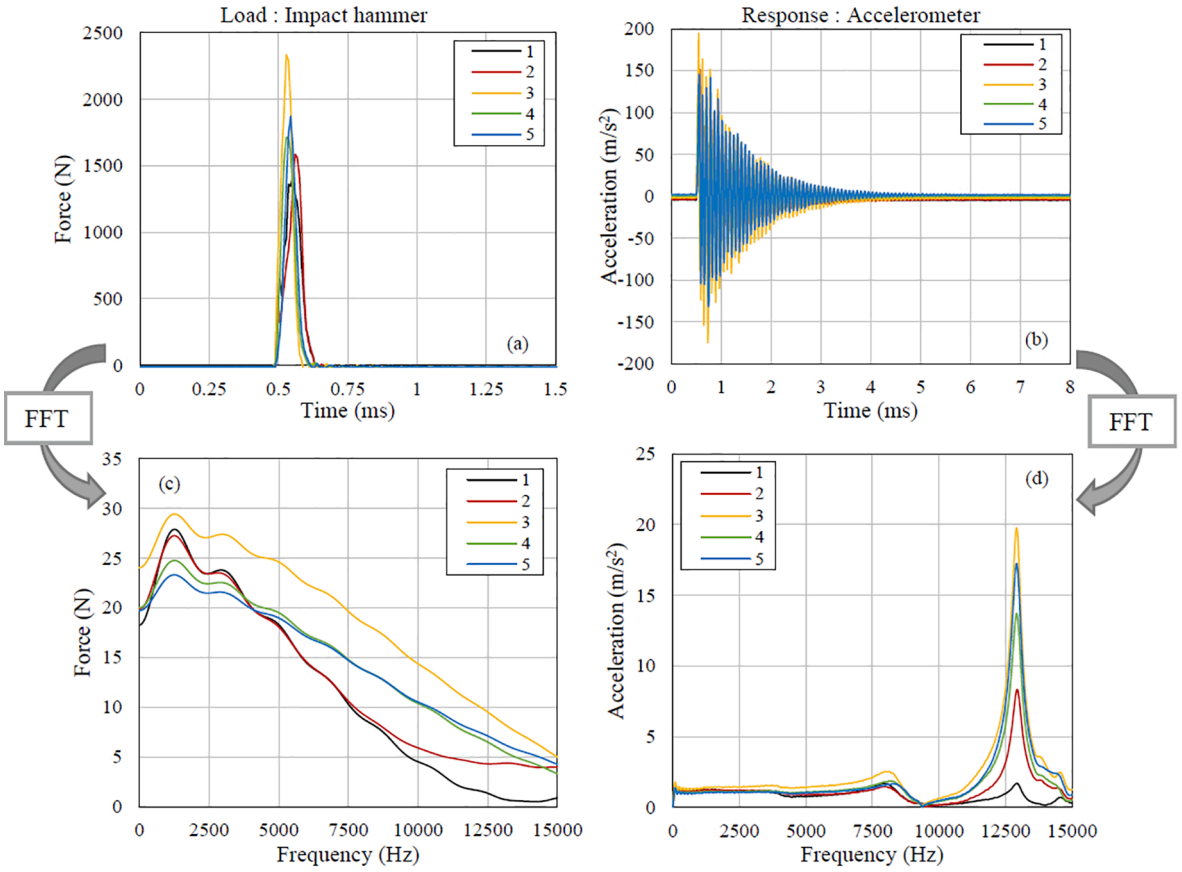

Fig. 4. Dynamic testing of complex modulus. Experimental data (five hits) for specimen 4 of ETS20_G100_D100 at –20 °C. (a) force in time domain, (b) acceleration in time domain, (c) force in frequency domain, (d) acceleration in frequency domain.

methodology developed by Carret et al. in previous works [21–24], an automated impact hammer equipped with a load cell (PCB model 086E80) was employed as an external input to generate standing waves inside the specimens (Fig. 3). The order of magnitude of the maximum strain in the specimen induced by the impact was of about 0.1 μm/m [23]. To achieve free boundary conditions, the specimens were placed on a soft foam during the test. An accelerometer (PCB model 353B15) was used to record the vibratory response of the specimens. Both the impact hammer and the accelerometer were connected to a signal conditioner (PCB model 482C15), connected as well to a data acquisition device (NI USB-6356), and finally connected to a computer (Fig. 3).

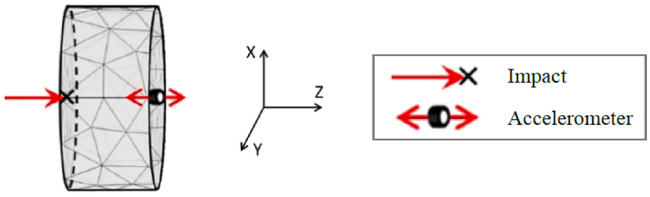

Fig. 6. Example of the finite element mesh, accelerometer and impact hammer positions, and boundary conditions used for the FEM calculation of the FRFs.

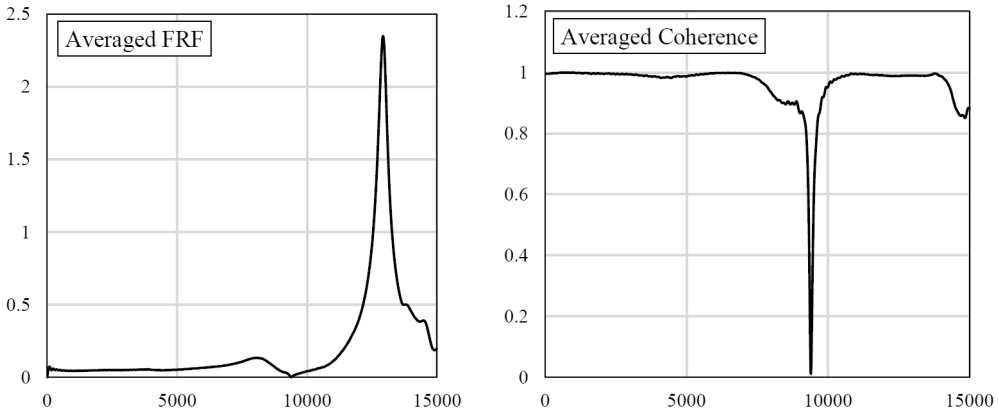

Fig. 5. Average of dynamic testing data in the frequency domain obtained for specimen 4 of the group ETS20_G100_D100 at –20 °C: (left) frequency response function; (right) coherence function.

Only the longitudinal vibration mode was considered in this study. The impact was applied at the center of one of the flat faces of the disc specimens, and the accelerometer recorded the signal at the center of the opposite face (Fig. 3).

The test temperatures used were the same as for the ITSM tests, –20, 0, and 20 °C, always conditioning the specimens for 4 h. The signals were recorded with a sampling rate of 1 MHz using an application specially designed for this purpose, which was developed with MATLAB software. The recording duration of the signals was adjusted for each test temperature to correctly record the vibrational response, taking into account the damping variation with temperature. Five impacts were applied at each temperature and the respective applied forces and accelerations were recorded for reliability purpose. An example of the experimental data is shown in Fig. 4 for the specimen 4 of group ETS20_G100_D100 at –20 °C.

For each temperature, the experimental data were transformed from the time domain to the frequency domain using Fast Fourier Transforms (FFT). As shown in Fig. 4, the energy spectrum of the impacts went up to around 15 kHz in the frequency domain. Therefore, the Frequency Response Functions (FRFs) were calculated from 1 Hz to 15 kHz, in steps of 1 Hz, averaging the results of the impacts using Eq. (3) [25]:

$$H(f) = \frac{\overline{Y(f)\cdot X^*(f)}}{\overline{X(f)\cdot X^*(f)}} \tag{3}$$

Where H means the FRF, Y means the FFT of the measured acceleration, X means the FFT of the applied force, X^* means the complex conjugate of the applied force and the bar above indicates the arithmetic average of the impacts. A coherence function was used to check the quality of the measurements. The results range from 0 to 1 where a value of 1 indicates that the response is fully explained by the impact, while a decreasing value means that something has disturbed the test. The FRF and the coherence function for specimen 4 of group ETS20_G100_D100 at –20 °C are shown in Fig. 5. The quality of the measurements was confirmed considering that all tests showed an indicator very close to 1, except for frequencies ranging from 9000 to 9500 Hz, which showed significant interferences in the results.

Then, the finite element method (FEM) was used to simulate the IR tests, assuming a linear viscoelastic behavior independent of the frequency ($E^* = E.e^{i\varphi}$) and free boundary conditions (Fig. 6), following the same procedure explained in depth in the research carried out by Carret [26].

The numerical FRFs were calculated by solving the following three-dimensional equation, Eq. (4), of motion in the frequency domain at the selected frequencies:

$$-\rho\omega^2\boldsymbol{u} - \nabla\cdot\sigma = 0 \tag{4}$$

Where ρ means the bulk density of the material, ω is the angular frequency, $\mathbf{u}$ is the vector of displacement, ∇ is the gradient tensor operator and σ is the Cauchy stress tensor. It is assumed free boundary conditions to solve Eq. (4), except at the point of impact where a cyclic load $e^{i\omega t}$ is applied in the impact direction. Following this method, for each tested temperature, the value of the norm of the complex modulus (E) was back-calculated so that the the first resonance frequency of the experimental and of the numerical FRFs match. The value of the phase angle (φ) wat not back-calculated to simplify the procedure and it was set to 0.5° considering the tests were performed at low temperatures. Carret et al. [22] showed that the value of Poisson's ratio has minimal influence on the numerical calculation of FRFs and that the norm and phase angle of the complex modulus can be obtained easily from the FRF at each temperature.

4.2.3. Cyclic tension–compression test (TC) on cylindrical specimen

The linear viscoelastic behavior of bituminous materials is commonly characterized using cyclic TC tests, in order to measure the complex modulus at various temperature and frequencies. In this study, the TC tests were done only on the original RAP source, with a NMS of 20 mm. The specimen tested had a height of 150 mm and a diameter of 75 mm, and was obtained by coring a 150 mm diameter SGC specimen at 100 gyrations.

Sinusoidal cyclic axial loads were applied by using a hydraulic press in a controlled deformation mode with an amplitude of about 50 μm/m. A load cell measured the axial tension, while the axial deformation was obtained from the average of the three strain gauges placed at 120 °. Finally, the radial deformation was derived from two non-contact sensors. The test was performed at 8 temperatures (–30, –23, –14, –4, 5, 15, 24 and 34 °C) and at 7 loading frequencies (0.01, 0.03, 0.10, 0.30, 1.00, 3.00 and 10 Hz). The detailed test set-up is shown in Fig. 7.

The experimental results obtained from the test were analyzed through the linear viscoelastic model 2S2P1D (2S: two Springs, 2P: two Parabolic elements, 1D: one Dashpot). The 2S2P1D model is explained in details in previous researches [26–28].

4.3. Failure behavior characterization

4.3.1. Indirect Tensile strength (ITS)

The ITS test was carried out according to ASTM D6931 at ÉTS, and according to EN 12697–23 at UDC. This test measures the tensile strength developed along the vertical diameter plane of the specimen subjected to a compressive load (Fig. 9), using Eq. (5) as follows:

$$ITS = \frac{2\cdot P}{\pi\cdot D\cdot t} \tag{5}$$

Where ITS means the tensile strength, P means the maximum load, t means the height and D the diameter of the tested specimen. The test was

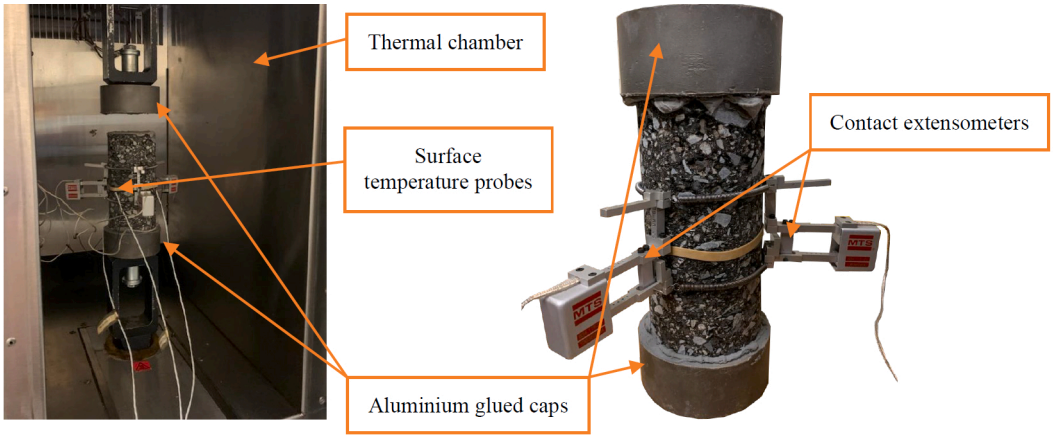

Fig. 7. Specimen before (left) and after (right) tension–compression test.

Fig. 8. Detail of SCB specimens prior to testing.

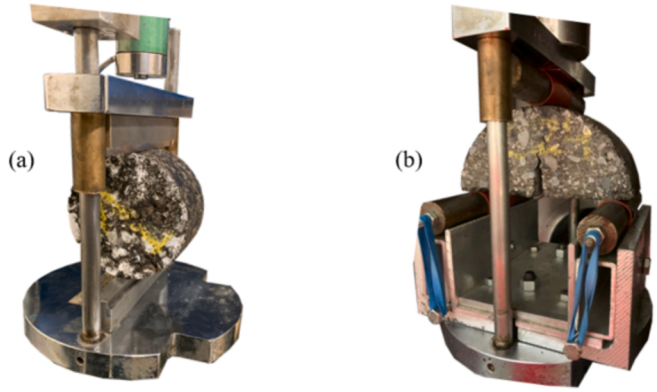

Fig. 9. (a) Detail of specimen 1 of group ETS20_G100_D100 after performing ITS test; (b) Detail of a semi–circular specimen prepared with RAP 0/5 after performing the SBC test.

performed on all specimens manufactured with a diameter of 100 mm, both those compacted with 100 and 200 gyrations of SGC, and the Marshall specimens; with the three NMS of RAP in each case. In all cases, the test temperature of 15 °C was used, after a conditioning period of 4 h, according to the European standard EN 12697–23.

4.3.2. Semi-circular bending test (SCB)

The SCB test was conducted in accordance with ASTM D8044–16. Twenty–four semi–circular specimens with a diameter of 150 mm and a thickness of 58 ± 1 mm were prepared from 3 specimens of 150 mm diameter compacted with 100 gyrations of SGC. The three NMS of RAP were used. A 25 mm notch parallel to the vertical axis was made in all of them. Fig. 8 shows the prepared specimens, ordered from left to right, eight prepared with RAP 0/5, eight with RAP 0/10, and eight with RAP 0/20.

Analogously to the previous tests, the selected test temperatures were –20, 0, and 20 °C, and the specimens were placed in a climatic chamber for conditioning for 4 h prior to each test. The specimens were positioned on a three-point bending test device inside the climatic chamber. The device has at the ends two 25 mm cylindrical supports separated by a length of 127 mm. To reduce friction, polytetrafluoroethylene strips were placed between the specimen and the test supports (Fig. 9). A monotonic displacement of 0.5 mm/min was exerted on the top center line of the specimen while a data acquisition system simultaneously recorded the load and vertical displacement. A preload of 45 ± 10 N was applied to the specimens prior to testing for a maximum of 30 s to ensure contact. Considering that only one notch size was used, the maximum load (*Pmax*) reached before failure, and the strain energy to failure (*U*) were calculated and compared for each mixture and temperature.

$$U = \sum_{i=1}^{n}(u_{i+1} - u_i) \times P_i + \frac{1}{2} \times (u_{i+1} - u_i) \times (P_{i+1} - P_i) \quad (6)$$

Where P_i means the applied load (kN) at the i load step application, and u_i means crosshead displacement (m) at the i step.

5. Results and discussion

5.1. Effect of nominal maximal size of RAP on volumetric properties

Table 3 summarizes the volumetric properties of all the mixtures studied. First, the ρ_m obtained for the mixtures with each type of RAP are shown. In addition, Table 3 also presents the calculated air void contents before ($V_{a,0}$) and after curing (V_a), for each specimen group studied. The values in Table 3 show the average value of all specimens prepared from each group. The variation of the air void contents was measured by the standard deviation of the results from the specimens in each group, indicated as a sub–index next to each value in Table 3.

From Table 3, it can be seen that the air void content increases by about 2% between the values before and after curing. This result was expected, since this increase corresponds to the evaporation of water during curing, and the dosage used in all the mixtures was the same. It is interesting to note that the specimens compacted with a Marshall hammer showed a greater increase, around 4%. In other papers on cold mixes, it was seen that this compaction was not the best suited for CRM in part because it is linked with a loss of material during its execution [18].

The SGC allows monitoring the evolution of compaction with the number of cycles by recording the heights throughout the process. Thus,

Table 3
Air void contents and respective standard deviations, before and after curing, according to the RAP and compaction method used.

	RAP source and NMS							
	ETS20 (ρ_m = 2517.07 kg/m^3)		ETS10 (ρ_m = 2507.60 kg/m^3)		ETS5 (ρ_m = 2501.68 kg/m^3)		UDC22 (ρ_m = 2419.22 kg/m^3)	
	$V_{a,0}$ (%)	V_a (%)	$V_{a,0}$ (%)	V_a (%)	$V_{a,0}$ (%)	V_a (%)	$V_{a,0}$ (%)	V_a (%)
G100_D100	10.5 $_{0.5\%}$	12.6 $_{0.4\%}$	10.6 $_{0.4\%}$	12.7 $_{0.3\%}$	11.9 $_{0.3\%}$	13.9 $_{0.2\%}$	19.6 $_{1.2\%}$	21.4 $_{1.1\%}$
G100_D150	9.6 $_{0.0\%}$	12.0 $_{0.02\%}$	10.7 $_{0.1\%}$	12.8 $_{0.2\%}$	11.3 $_{0.1\%}$	13.8 $_{0.2\%}$		
G200_D100	8.1 $_{0.3\%}$	10.2 $_{0.5\%}$	8.6 $_{0.1\%}$	10.7 $_{0.3\%}$	8.6 $_{0.1\%}$	10.7 $_{0.2\%}$	16.6 $_{0.3\%}$	18.6 $_{0.2\%}$
M50_D100	16.1 $_{0.7\%}$	20.2 $_{0.7\%}$	17.7 $_{0.3\%}$	21.6 $_{0.3\%}$	19.4 $_{0.3\%}$	24.2 $_{0.3\%}$		25.5 $_{0.3\%}$

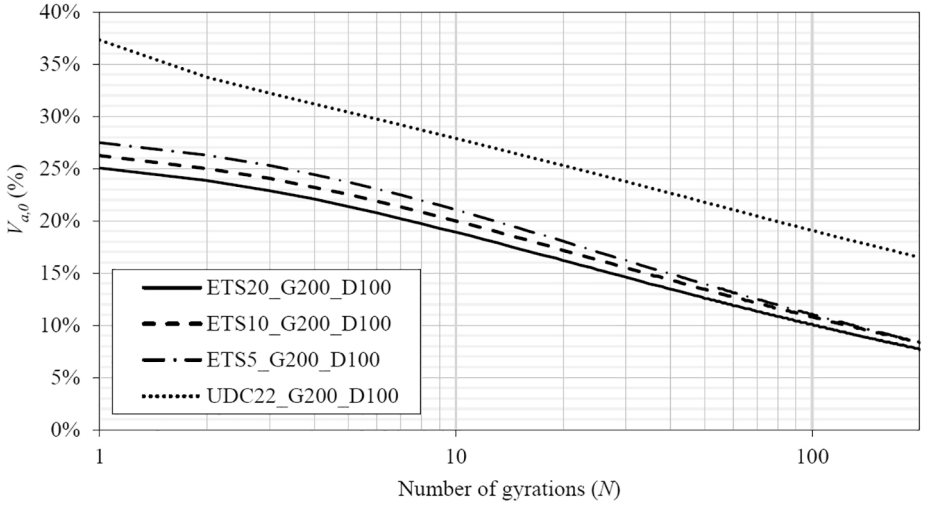

Fig. 10. Average compaction curves of mixes with different NMS.

Fig. 10 shows the evolution of the air void content (before curing, i.e., $V_{a,0}$) of the four mixes studied, using each type of RAP. Each line in Fig. 10 corresponds to the average of at least 3 specimens prepared all with the same mass of mixture, using 100 mm molds and compacted up to 200 gyrations.

The variation in the NMS of the RAP affected the ρ_m of the three mixes studied at ÉTS (Table 3). The reduction of the NMS resulted in a decrease of the ρ_m. This same trend is observed in the compaction curves in Fig. 10 for the mixes produced at ÉTS. When compaction begins (first gyration), the lowest air void content was that of the mixture using RAP with NMS of 20 mm, followed by that of 10 mm and then 5 mm, with values of 25.1%, 26.2%, and 27.5%, respectively. These differences were reduced once the 200 gyrations were completed, with values of 8.1%, 8.6%, and 8.6%, respectively. This trend towards more homogeneous results of voids with the increasing number of gyrations could be appreciated by looking at the slightly different slopes of the compaction curves in Fig. 10. This higher density achieved by the mixes with RAP 0/20 is attributed, on the one hand, to the higher density of coarser particles, which were extracted in the mixes with lower NMS, and on the other hand, to a particle size distribution that included all grain sizes, which give a better adjustment among particles from the beginning of the compaction. Even if the same mass was used for all mixes, the initial height recorded by the compactor was always lower for the mixture using the RAP with a NMS of 20 mm compared to the other NMS. However, the slopes of the curves indicated that the mixtures with the lowest NMS showed a higher rate of air void content reduction, reaching comparable compaction levels for a higher number of cycles. Thus, the air void contents obtained in mixes ETS5_G200_D100 and ETS10_G200_D100 were the same, and only 0.5% higher than that of mix ETS20_G200_D100.

The mixture prepared at UDC, with a different RAP source, exhibited the lowest ρ_m of all. Considering the particle size distributions of the RAP 0/20 from ÉTS and RAP 0/22 from UDC, there was a clear lack of intermediate-sized particles and a higher content of fine particles in this latter mix (Fig. 2). The lack of intermediate sizes led to worse inter-particle packing. The increase in filler generally leads to an increase in the workability of the mixes, while the compactability is usually reduced, as concluded in other articles discussing the influence of particle size in CRM [12]. Despite this worse initial fit, and consequently higher initial air void content, the rate of air voids reduction (compactability) was similar to that of the previous mixes, as can be seen from the slope of the compaction curve. The SGC internal angles at ÉTS and UDC were slightly different due to the respective specifications, however, the differences obtained in volumetric properties are mainly due to the particle size distribution and the proper inter–particle fit.

As expected, the air void contents of specimens prepared using Marshall compaction were higher than those obtained using the SGC. The trend in air void contents was still analogous for the different mixes. The decrease in the NMS of RAP used in the mixes studied at ÉTS led to an increase in air void content after compaction. The mix compacted in the UDC, using the RAP 0/22, was again the one with the highest air void content.

5.2. *Effect of NMS, temperature, air void content and compaction method on stiffness*

5.2.1. *Indirect Tensile stiffness modulus*

The ITSM results as a function of air void content are shown in Figs. 11 and 12. For both figures, three plots are displayed, one for each test temperature (–20, 0 and 20 °C). Fig. 11 shows the results for the groups compacted with 100 gyrations of SGC and Fig. 12 shows the results for those compacted with the Marshall hammer. In all plots, the results obtained for mixtures using the three considered NMS of RAP are specified. To simplify the comparison between graphs, the vertical axis of each graph was normalized by the average ITSM at each temperature.

In both Figs. 11 and 12, the increase in test temperature resulted in an overall decrease in ITSM results, due to the thermal sensitivity of all bituminous materials. At low temperatures (Fig. 11a and 12a) the ITSM results showed less dispersion and depended more clearly on the air void contents. In Fig. 11b and 11c, corresponding to 0 °C and 20 °C, the normalized ITSM results do not show a clear trend with the change in air void contents, where variations due to repeatability over two specimens appear predominant. The results are again scattered in the graphs of Fig. 12b and 12c, but in this case, a slight improvement in the *ITSM*—V_a correlation can be observed compared to those in Fig. 11b and 11c. This was because the air void contents of Marshall specimens represented in

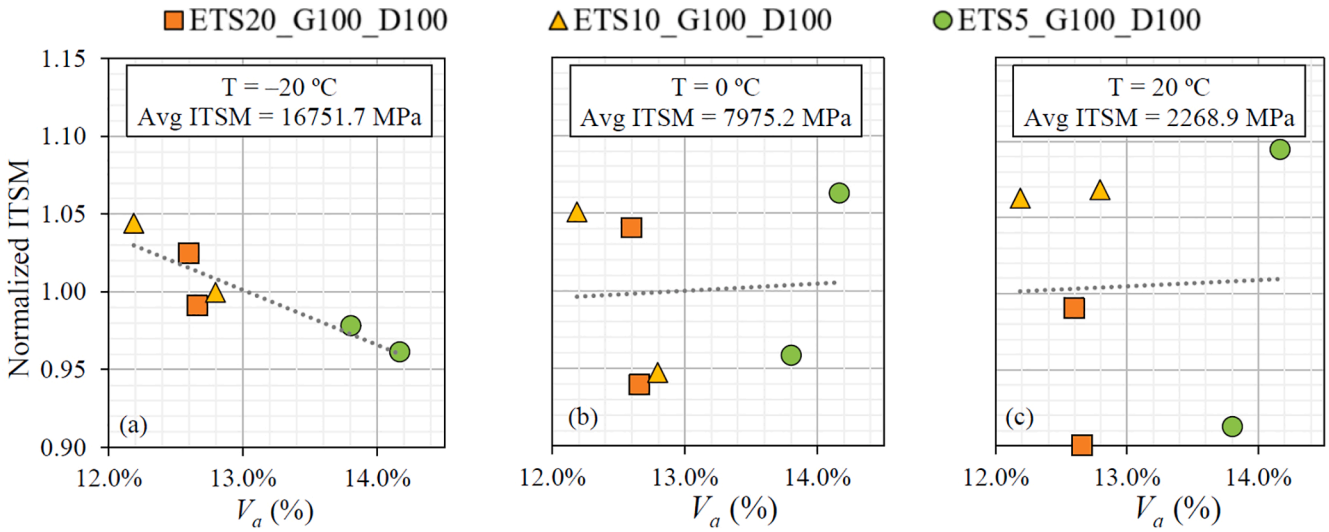

Fig. 11. Normalized ITSM of specimens prepared with different NMS of RAP, 100 gyrations of SGC, at different temperatures: a) –20 °C, b) 0 °C, c) + 20 °C.

Fig. 12 showed a greater variation from one mixture to another. Indeed, the variation range of air void content increases from 2% with SGC to 5% with Marshall compaction. Since for the Marshall specimens there were significant variations in V_a and variation of the RAP NMS, it is not clear what was the main cause of the variation in the stiffness results. For the SGC specimens, the variability of V_a was lower and the variations of NMS did not show a clear trend. As expected, a general decrease in stiffness was observed in specimens with higher air void content.

Concerning the NMS of RAP in the mixtures, Fig. 11 showed a slightly better performance for the mixture using NMS of 10 mm, however, the trend was not clear. The mixes with NMS of 10 and 20 mm showed rather similar air void contents, and from Fig. 11a and 11b there was no clear difference due to the RAP NMS. In Fig. 12, the highest ITSM results at all temperatures were those of the mixture using NMS of 20 mm, which happened to also have the same air void content. It was considered that for each temperature, the trend of decreasing ITSM was caused mainly by the increase in air void content rather than by the influence of the NMS of the RAP (Fig. 12). Temperature remained the factor with the greatest impact, with an average decrease in ITSM results of more than 50% when the temperature increased from –20 °C to 0 °C, and more than 70% when temperature increased from 0 °C to 20 °C.

Table 4 shows the averages of all the ITSM results ($\overline{ITSM}$) obtained for each NMS, at each temperature for both compaction methods. In addition, normalized standard deviations (SD / $\overline{ITSM}$) were calculated by dividing each standard deviation, SD, by the corresponding mean value, $\overline{ITSM}$.

As concluded from the normalized ITSM in Figs. 11 and 12, the scattering of the ITSM results increased as the temperature did, thus showing an overall increase of the relative standard deviations in Table 4. Marshall-compacted specimen groups showed a certain tendency to decrease the ITSM with decreasing NMS of RAP, however, as discussed before, it was considered to be mainly caused by the increasing air void contents. The same conclusion was also drawn in view of Fig. 11b and 11c corresponding to gyratory-compacted specimens. In this case, the air void content variations were considerably smaller, and still no clear variation pattern of ITSM was observed with the NMS of RAP.

5.2.2. *Complex modulus evaluated with dynamic IR test*

When calculating the numerical FRFs at the three different temperatures, it was noted that the resonance frequency and amplitude decreased as the temperature increased, showing changes in the properties of the material due to the viscoelastic behavior of the specimens. This made it difficult to calculate the stiffness modulus from the dynamic

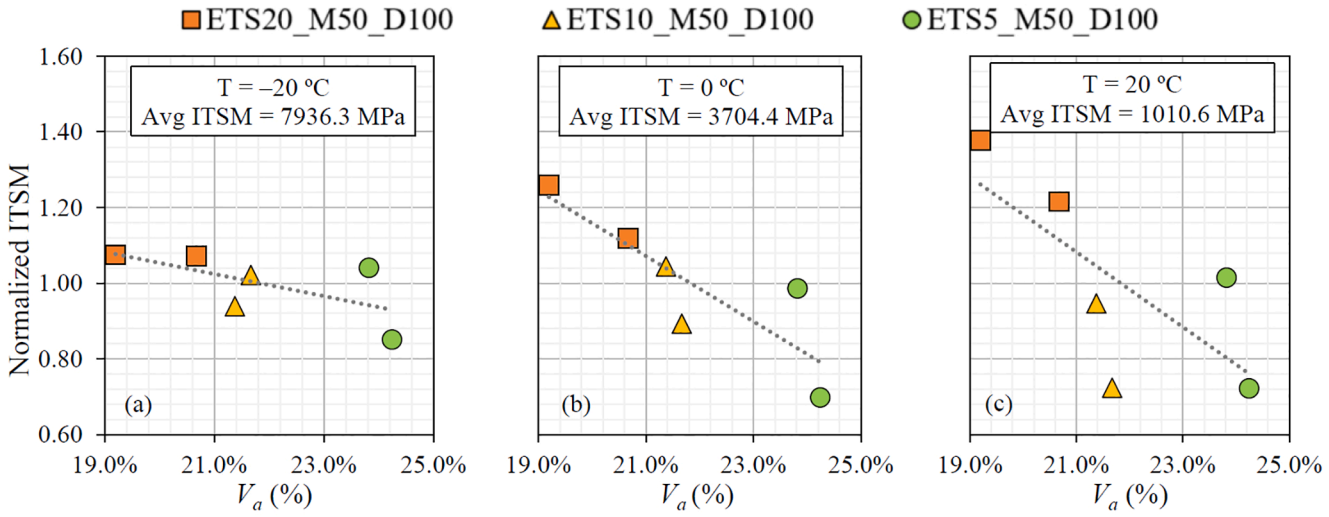

Fig. 12. Normalized ITSM of specimens prepared with different NMS of RAP, 50 blows of Marshall hammer, at different temperatures: a) –20 °C, b) 0 °C, c) + 20 °C.

Table 4
Average and normalized standard deviations (SD) of ITSM results.

	Test temperature					
	–20 °C		0 °C		20 °C	
	$\overline{ITSM}$	SD /$\overline{ITSM}$	$\overline{ITSM}$	SD /$\overline{ITSM}$	$\overline{ITSM}$	SD /$\overline{ITSM}$
R20_G100_D100	16887.6	3.60%	7896.2	6.42%	2134.0	6.82%
R10_G100_D100	17119.5	3.47%	7968.4	7.25%	2406.5	3.59%
R5_G100_D100	16247.9	1.49%	8060.9	6.63%	2266.1	11.59%
R20_M50_D100	8520.6	9.82%	4405.6	8.25%	1310.2	9.51%
R10_M50_D100	7780.1	6.48%	3588.4	9.01%	843.8	17.08%
R5_M50_D100	7508.0	11.95%	3119.1	20.14%	877.7	19.48%

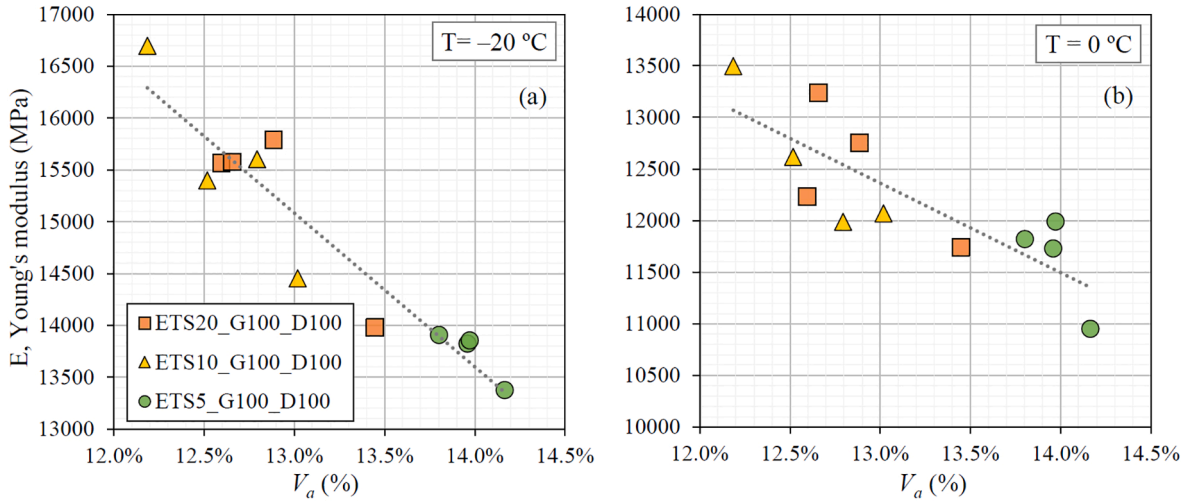

Fig. 13. Complex modulus determined by dynamic IR tests of specimens prepared with different NMS of RAP, 100 gyrations of SGC, at different temperatures: a) –20 °C; b) 0 °C.

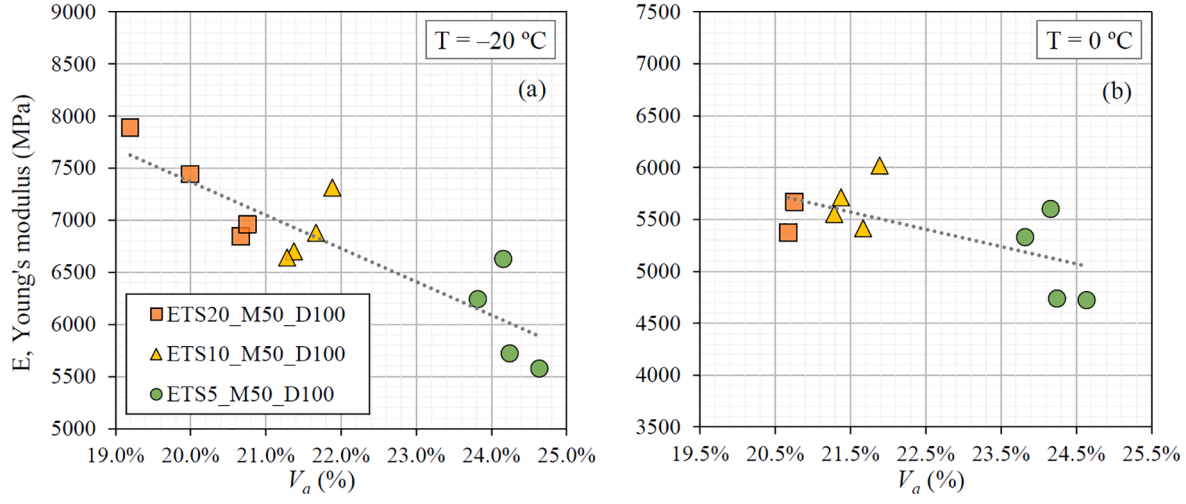

Fig. 14. Complex modulus determined by dynamic IR tests of specimens prepared with different NMS of RAP, 50 blows of Marshall hammer, at different temperatures: a) –20 °C; b) 0 °C.

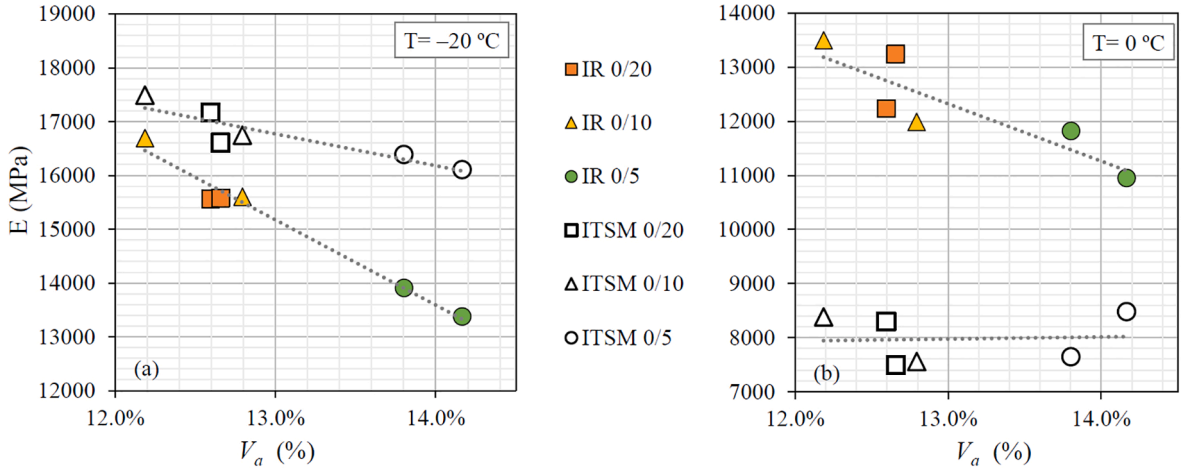

Fig. 15. ITSM and dynamic IR test results at 0 and –20 °C for the same SGC specimens.

IR tests performed at 20 °C without using a frequency dependent viscoelastic modelling of the material behavior. Consequently, Fig. 13 and Fig. 14 only show graphs with the results at –20 °C and 0 °C. Each point on the graphs represents the norm of the complex modulus result for each specimen related to its air void content.

As it is inherent to the viscoelastic behavior of the asphalt mixtures, the values of the norm of the complex modulus at 0 °C were lower than those at –20 °C by 18% on average for the SGC specimens, and by 20% for the Marshall specimens. However, from the graphs in Figs. 13 and 14, it is observed that the norm of the modulus not only varies with temperature, but also with the volume of air void in the mixes. The results with RAP 0/20 and 0/10 in Fig. 13 did not show clear general differences depending on the NMS, as those specimens have similar air void contents. However, for those specimens of both groups, those using RAP 0/20 showed slightly higher values of the norm of the complex modulus but the difference is not significant. In addition, the norm of the complex modulus of specimens with RAP 0/5 is lower than for the specimens of the two other groups, likely because of their higher air voids. Therefore, it can be concluded that an increase in air void content led to a decrease in the norm of the complex modulus. Although rather higher results were achieved in mixes with higher NMS, no trend was observable concerning the variations of the RAP max size, and the impact of air void content definitely appears more significant, as concluded from the ITSM results. Overall, the NMS could be a negligible factor.

5.2.3. *Comparison between ITSM and dynamic IR test results*

Since the test temperatures and specimens tested were the same between the ITSM and the dynamic IR tests, the results can be compared. These results are shown in Figs. 15 and 16, again related to the air void content of each specimen. The vertically aligned points on the graphs correspond to the results for the same specimen.

It was observed in the comparison in Fig. 15a and 16a that at –20 °C the ITSM results were on average 10.2% higher than those obtained with the dynamic IR tests for the SGC specimens. This average discrepancy rose to 18.7% for the Marshall specimens. The linear regression shows almost parallel lines between, confirming that both approaches measure the same effect of air void content to a first-order approximation.

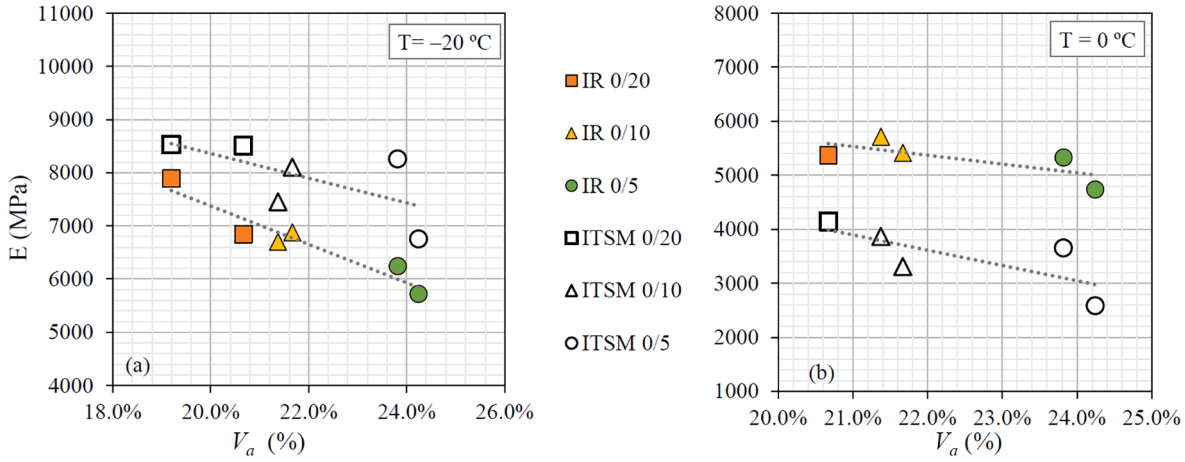

Fig. 16. ITSM and dynamic IR test results at 0 and –20 °C for the same Marshall specimens.

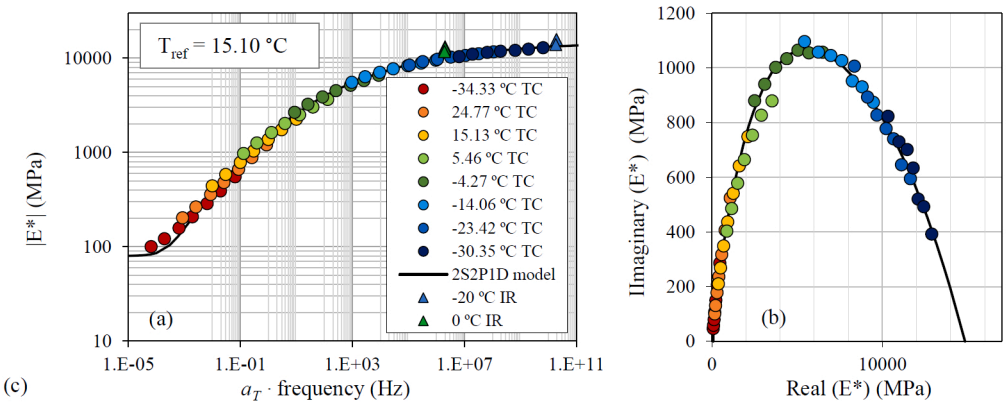

E_{00} (MPa)	E_0 (MPa)	k	h	δ	τ_E (s)	β	ν_{00}	ν_0	γ_{Ev}	τ_v (s)
80.00	14850.00	0.15	0.41	2.15	0.00	4603.00	0.12	0.19	150.00	3.48E-01

Fig. 17. Tension-compression test results, and 2S2P1D model simulation and constants to fit the test results: (a) master curve at 15.1 °C and results from dynamic IR tests; (b) Cole–Cole diagram; (c) constants of the model 2S2P1D.

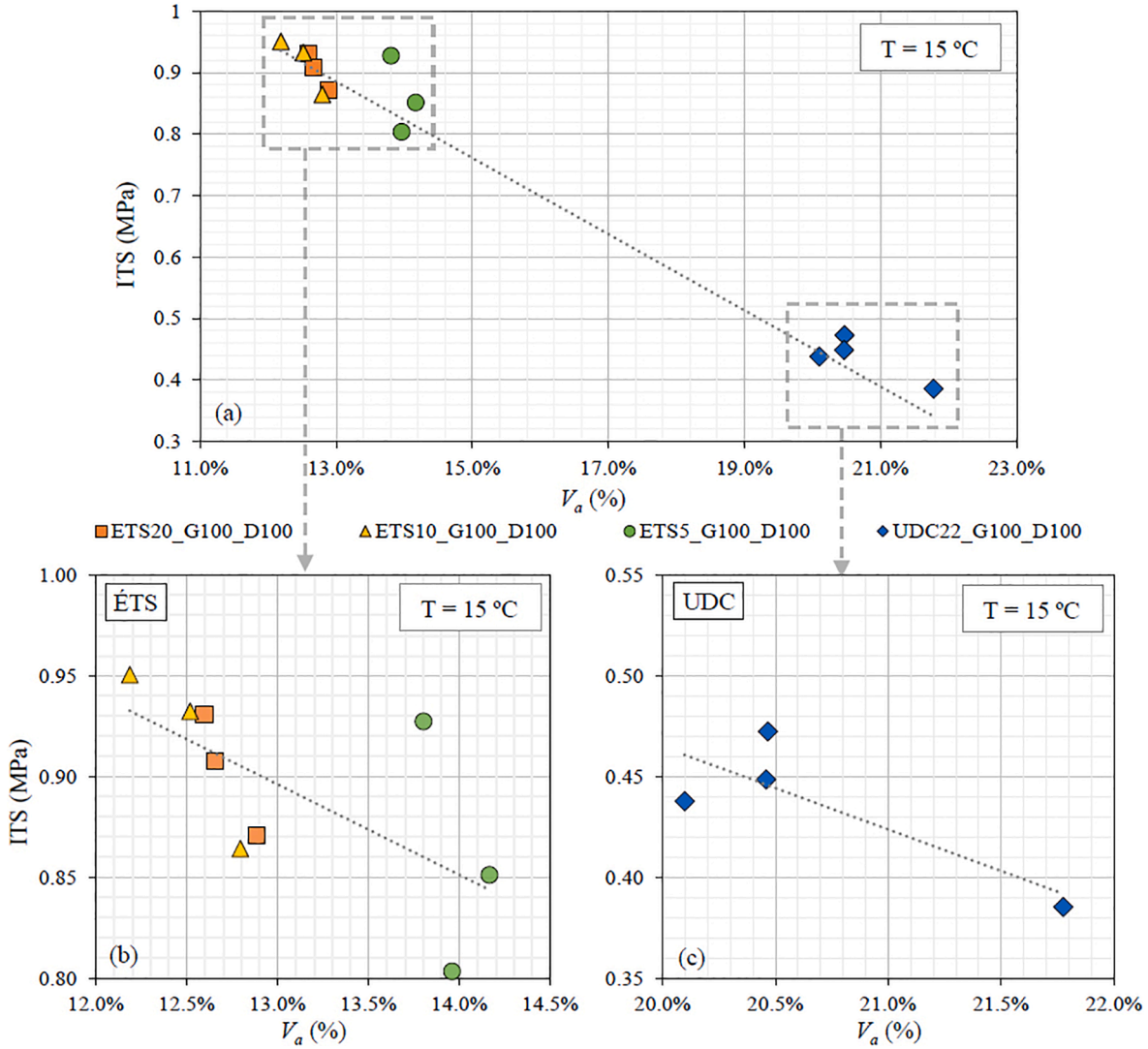

Fig. 18. Indirect tensile strength tests of specimens prepared with 100 gyrations of SGC: a) specimens prepared at ÉTS and UDC, b) specimens prepared at ÉTS, c) specimens prepared at UDC.

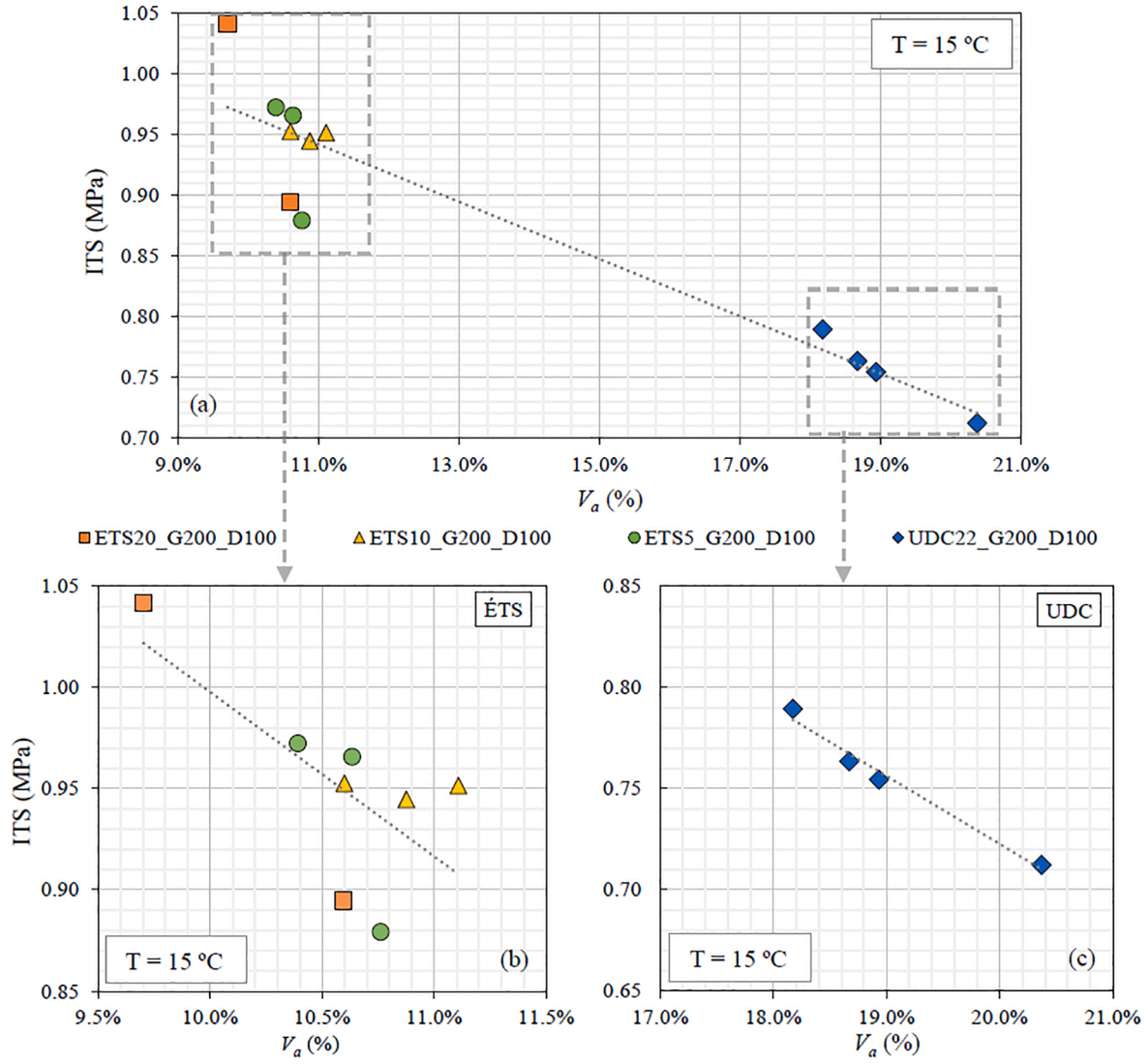

Fig. 19. Indirect tensile strength tests for specimens prepared with 200 gyrations of SGC: a) specimens prepared at ÉTS and UDC, b) specimens prepared at ÉTS, c) specimens prepared at UDC.

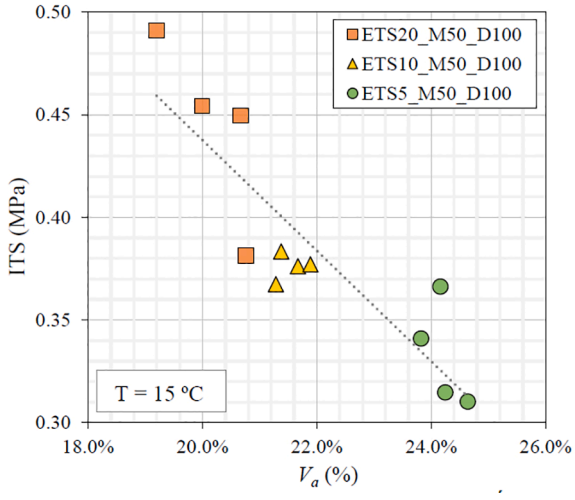

Fig. 20. Indirect tensile strength tests for specimens prepared at ÉTS using 50 blows of Marshall hammer.

However, at 0 °C the dispersion was greater, and in this case the ITSM results were on average 34.7% lower for the SGC specimens (Fig. 15b) and a 37.0% lower for Marshall specimens (Fig. 16b). Indeed, the IR approach usually yields clearer results with less viscous materials, especially mixtures at very low temperatures. A clear relationship between the tests could not be established for all temperatures, but it confirmed the relation with the degree of compaction, i.e., the volume of air voids, in all cases.

5.2.4. *Comparison between complex moduli obtained with TC and dynamic IR tests*

The results of the complex moduli determined using the tension–compression test are represented in Fig. 17, together with those obtained from the dynamic IR tests. Good continuity of the measurements made with TC tests at various temperatures can be seen in the Cole–Cole plot (Fig. 17b), demonstrating that the material is rheologically simple and that the time–temperature superposition principle applies. The constant parameters used in the Williams–Landel–Ferry (WLF) equation [29] were $C_1 = 17.69$ and $C_2 = 136.23$. Using this equation it was possible to obtain the shift factors (a_T) needed to calculate the reduced frequencies and be able to generate the master curve of Fig. 17a, at the reference temperature of 15.10 °C. Thus, Fig. 17a shows the

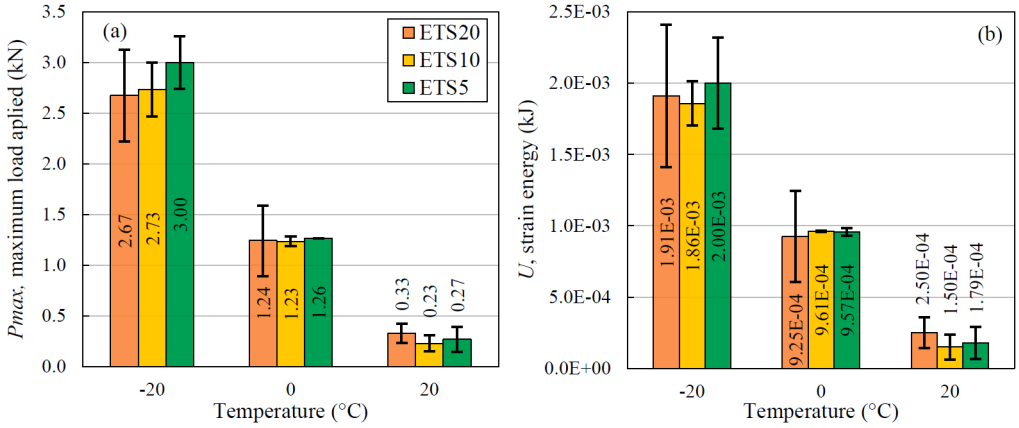

Fig. 21. Results in the SCB tests for the CRMs with the three NMS of RAP: a) Maximum load, P_{max}; b) strain energy to failure, U.

master curve at the reference temperature, the modulus results from the IR test of the same mix for the corresponding reduced frequencies, and the 2S2P1D model fitted to the real TC test results. It is observed that the test results fit the 2S2P1D model very well. In Fig. 17c, the adjusted parameters of the model for the real TC test results are shown.

In Fig. 17a it can be seen that the values of the norm of the complex modulus obtained from the dynamic IR tests were higher than the values obtained with the TC test, and those predicted by the 2S2P1D model, for the same reduced frequencies. These differences were smaller with higher frequencies (and lower temperatures). Thus, the complex modulus results from the dynamic IR tests at 0 °C were 23% higher than those of the TC tests, while they were only 14% higher at –20 °C. This effect was expected, and was also observed in other studies [21,22]. This is due to the fact that the levels of deformation applied in each test are different (about 50 μm/m for the tension–compression tests versus about 0.1 μm/m for the dynamic tests), and asphalt mixtures have a performance highly dependent on the level of deformation [30,31]. Nevertheless, the shift factors applied to IR results, calculated from WLF modelling of TC results, appeared to fit well, suggesting that the temperature sensitivity of mixtures could be equally measured to a first-order approximation with both methods.

Considering that IR dynamic tests have the great advantage of being inexpensive and simple to perform, and can provide the complex AM modulus over a wide range of frequencies and temperatures with good accuracy from simple calculations, they are considered a promising alternative to traditional T-C tests.

Furthermore, it is known from the findings of other researchers that CRMs exhibit stress-dependent mechanical behavior [32,33]. Therefore, the combination of stiffness modulus tests at various temperatures, frequencies and confining pressures is considered a very interesting issue for further research.

5.3. *Effect of NMS, air void content, and compaction on Indirect Tensile strength*

All the specimens with a diameter of 100 mm produced in this study were subjected to ITS testing, including those previously tested with ITSM and complex modulus by dynamic IR method. Figs. 18, 19, and 20 show the ITS results of each specimen, once again related to its air void content. The results of the graphs in Fig. 18 refer to specimens compacted with 100 gyrations of SGC, those in Fig. 19, to those compacted with 200 gyrations of SGC, and that in Fig. 20, to those compacted with 50 blows of Marshall hammer. Regarding Figs. 18 and 19, both specimens manufactured at ÉTS and UDC are included in the graphs.

Fig. 18a showed a clear influence of air void contents on the ITS results for the four mixtures compacted with 100 gyrations of SGC. It was observed that the trend of decreasing ITS values with increasing air void contents was similar for both the specimens prepared at ETS and UDC. Considering the mixtures using RAP with NMS of 20 and 10 mm in Fig. 18b, they showed similar air void contents, and no clear trend of ITS results with the variation of NMS was observed, as was the case for the norm of the complex modulus (Fig. 13).

Regarding the results for the specimens compacted with 200 gyrations (Fig. 19), again there was a tendency for the results to decrease with increasing air void content; and this tendency was particularly noticeable in the case of Fig. 19c, where it was fairly linear. It is worth noting that after 200 gyrations of SGC (Fig. 19b), the mix with NMS 20 mm showed an air void content similar to that of the other two mixes than when 100 SGC gyrations were applied (Fig. 18b), and also exhibited somewhat higher ITS results (Fig. 19b), but the difference was not really significant. It was already seen in the compaction analysis that the ÉTS mixes with 5 mm of NMS had better compactability (higher slope of the compaction curve), and that after 200 turns their air void content was comparable to that of the ÉTS mixes with 10 mm of NMS. Thus, in all Figs. 18, 19, and 20, the overall dependence of the ITS results on the air void content is remarkable, whereas the influence of NMS of RAP based on the presented results was not measurable.

Fig. 18b, 19b, and 20 might suggest that higher NMS leads to higher ITS results. However, from Fig. 18a and 19a, it can be observed that the mix prepared at UDC, which had the highest NMS (as well as RAP from different origin), presented the lowest ITS results, which was considered to be due to its higher air void content compared to those prepared at ÉTS. Therefore, air void content appears as a predominant factor for failure behavior compared to the NMS of the RAP used.

5.4. *Effect of NMS and temperature on failure behavior evaluated with Semi–circular bending test*

The specimens used for the SCB tests were prepared from 150 mm diameter gyratory specimens, compacted with 100 gyrations, and their volumetric properties are shown in Table 3.

Fig. 21 shows the maximum loads (P_{max}) and strain energies to failure (U) achieved on average on the SCB test for the mixtures studied at ÉTS at the temperatures considered. The bars of the graphs in Fig. 21 represent the average results of 4 specimens in each case, showing also their standard deviations.

From the Fig. 21, it can be observed that mixtures with lower NMS of RAP had a slightly better behavior under cracking at lower temperatures, reaching the highest average values of P_{max} as well as U. Considering Fig. 21a, the differences of P_{max} average values obtained at 0 and 20 °C were not very significant, and the trend of P_{max} with the NMS of RAP was not clear; but at lower temperatures, such as –20 °C, when they are more stiff and brittle, it could be seen that the average P_{max} reached by the mixtures with RAP 0/5 was 9.8% higher than that of

the mixtures with RAP 0/10, and 12.2% higher than that of those with RAP 0/20. However, the variability of the results shown by the standard deviations makes the trends of P_{max} and U unclear in terms of the NMS of the RAP.

The influence of the mineral skeleton is greater with increasing temperature, due to the viscoelastic nature of CRMs. Thus, although the trends of the results in Fig. 21 were even less clear at 0 °C and 20 °C, it seems that at 20 °C the tendency was for the mixes using RAP with 20 mm of NMS, which have greater internal friction between aggregates, to perform better, although with minor differences. The average differences between the results were relatively higher at low temperatures, presenting better cracking behavior the mixes with lower NMS of RAP. However, as expected when comparing the effect of NMS and temperature together, the effect of temperature always had a significantly greater effect, with a clear worsening of the cracking behavior with increasing temperature.

6. Conclusions

In this study on CRMs, the impact of the type of RAP used on both compactability and mechanical performance was studied. RAP from two different origins was used, also varying the NMS of one of them. First, volumetric properties were studied by fixing a mix design, and using two laboratory compaction methods. Tests to evaluate stiffness and failure behavior were then performed at different temperatures. Mechanical properties results were compared and analyzed according to RAP properties, compaction procedure, air voids content and temperature. The main conclusions drawn from the study are summarized as follows:

- The particle size distribution of the RAP strongly influenced the volumetric properties of the CRMs. For the mixes produced at ÉTS with the same RAP source, a reduction in the NMS resulted in a reduction of the maximum densities. Mixtures using lower NMS of RAP also required higher compaction energy to reach similar air void contents as mixtures with a higher NMS of RAP. The compaction curves were reasonably parallel in all cases, thus the density obtained, after the same number of SGC gyrations, significantly depended on the density from the initial cycle. A complete gradation, presenting all aggregate sizes in their right proportion, was related to a better initial adjustment between particles and, consequently, to higher densities obtained. The RAP used in the UDC, coming from a different source, even presenting higher NMS, showed a lack of intermediate particles. The maximum density of this mixture was lower and showed significantly higher air void content after the same number of SGC gyrations.
- ITSM, and dynamic IR tests exposed the dependence of the stiffness moduli on not only temperature and frequency, but also high dependence on the air voids content. This dependence was especially noticeable for lower temperatures, showing higher stiffness when the air void contents were lower. The influence of the NMS of the RAP was minor and the trend was also unclear.
- Dynamic IR tests proved to be a promising alternative to traditional TC tests for studying the linear viscoelastic (LVE) behavior of asphalt mixtures. Dynamic IR tests have the great benefit of being fast, inexpensive and non-destructive, and can determine the LVE behavior of asphalt mixtures over a wide range of frequencies and temperatures. The norms of the complex moduli resulted from the TC tests were slightly lower than those obtained with dynamic IR tests, due to the different strain level of the tests, and became smaller for higher frequencies. These results were in accordance with previous studies on the influence of the deformation level of asphalt mixtures. It is considered interesting to extend its application to CRMs with different geometries to verify its level of accuracy.
- The results of the ITS tests showed a significant influence of the air voids content compared to the variation in the NMS of the RAP. Mixes prepared in the ÉTS with the same RAP source, varying the NMS, had quite similar V_a and showed significant variability in the ITS results, with no clear trend in terms of the NMS. The mix prepared at UDC presented the lowest ITS values. This mix, despite having the highest NMS of RAP, showed the highest air void content, highlighting the major relevance of this parameter. The fracture behavior resulting from the SCB tests on mixtures with different NMS of RAP showed quite similar response between mixtures. At – 20 °C, the average results of maximum load and energy to failure using the lowest RAP NMS were slightly higher, and there was more variation between results. At 20 °C, the results were slightly higher in mixes using the highest RAP NMS, although there were smaller differences between mixes. However, the standard deviations obtained mean that trends were not entirely clear in terms of NMS.

With respect to the variation found in the results of mechanical behavior, the importance of adequate compaction of CRM was highlighted. The air void content of the mixes is an essential factor. Many specifications on CRM indicate certain strength requirements to be fulfilled by mixtures prepared with a certain compaction energy, but not all of them indicate the level of compaction to be achieved (as is the case of the current Spanish specification OC 40/2017, for example). Variations in the properties of the RAP, especially the grain size distribution, greatly influenced the maximum density and compactability of the mixtures. Therefore, specifying certain strength requirements in a design method must be linked to certain demands on the target compaction level, and not just the compaction energy to be applied. Further research should focus on the determination of grain size limits that allow obtaining the maximum possible density of the mixtures, thus improving compactability, reducing the volume of air voids, and consequently improving mechanical behavior.

Declaration of Competing Interest

The authors declare that they have no known competing financial interests or personal relationships that could have appeared to influence the work reported in this paper.

Acknowledgements

The authors would like to acknowledge funding for the project BIA2016-80317-R from the Spanish Ministry of Science and Innovation, with an associated pre-doctoral scholarship for the training of research workers (FPI) BES-2017-079633. The authors would also like to express their sincere gratitude for being awarded the INDITEX 2020 grant for pre-doctoral stays in foreign research centers, which has made it possible to carry out this research study. The corresponding author would like to thank, in addition to the co-authors, O. Baklouti, M. Beheshtighanad, T. Kakpo Edeme, M-A. Bérubé, S. Bibeau, and F. Bilodeau for their support and assistance in the laboratory work. An special acknowledgement to the Universidade da Coruña/ CISUG for funding the Elsevier's open access charge.

References

[1] F. Xiao, S. Yao, J. Wang, X. Li, S. Amirkhanian, A literature review on cold recycling technology of asphalt pavement, Constr. Build. Mater. 180 (2018) 579–604, https://doi.org/10.1016/j.conbuildmat.2018.06.006.
[2] S. Jain, B. Singh, Cold mix asphalt: An overview, J. Clean. Prod. 280 (2021) 124378, https://doi.org/10.1016/j.jclepro.2020.124378.
[3] T. Wang, F. Xiao, X. Zhu, B. Huang, J. Wang, S. Amirkhanian, Energy consumption and environmental impact of rubberized asphalt pavement, J. Clean. Prod. 180 (2018) 139–158, https://doi.org/10.1016/j.jclepro.2018.01.086.
[4] N. Thom, A. Dawson, Sustainable Road Design: Promoting Recycling and Non-Conventional Materials, Sustainability. 11 (2019) 6106, https://doi.org/10.3390/su11216106.
[5] F. Gu, W. Ma, R.C. West, A.J. Taylor, Y. Zhang, Structural performance and sustainability assessment of cold central-plant and in-place recycled asphalt pavements: A case study, J. Clean. Prod. 208 (2019) 1513–1523, https://doi.org/10.1016/j.jclepro.2018.10.222.

[6] G. Valdes-Vidal, A. Calabi-Floody, E. Sanchez-Alonso, Performance evaluation of warm mix asphalt involving natural zeolite and reclaimed asphalt pavement (RAP) for sustainable pavement construction, Constr. Build. Mater. 174 (2018) 576–585, https://doi.org/10.1016/j.conbuildmat.2018.04.149.
[7] A. Pakes, T. Edil, M. Sanger, R. Olley, T. Klink, Environmental Benefits of Cold-in-Place Recycling, Transp. Res, Rec. J Transp. Res. Board. 2672 (24) (2018) 11–19, https://doi.org/10.1177/0361198118758691.
[8] P. Orosa, I. Pérez, A.R. Pasandín, Short-term resilient behaviour and its evolution with curing in cold in-place recycled asphalt mixtures, Constr. Build. Mater. 323 (2022) 126559, https://doi.org/10.1016/j.conbuildmat.2022.126559.
[9] P. Orosa, L. Medina, J. Fernández-Ruiz, I. Pérez, A.R. Pasandín, Numerical simulation of the stiffness evolution with curing of pavement sections rehabilitated using cold in-place recycling technology, Constr. Build. Mater. 335 (2022), https://doi.org/10.1016/j.conbuildmat.2022.127487.
[10] A. Academy, Technical Guideline (TG2): Bitumen Stabilised Materials Southern African Bitumen Association (Sabita), Pretoria, South Africa, 2020.
[11] D. Perraton, G. Tebaldi, E. Dave, F. Bilodeau, G. Giacomello, A. Grilli, A. Graziani, M. Bocci, J. Grenfell, P. Muraya, M. Pasetto, K. Kuna, A. Apeagyei, D. Lo Presti, G. Airey, K.J. Jenkins, E. Hajj, M. Hugener, P. Marsac, Tests Campaign Analysis to Evaluate the Capability of Fragmentation Test to Characterize Recycled Asphalt Pavement (RAP) Material, in, RILEM Bookseries (2016) 965–976, https://doi.org/10.1007/978-94-017-7342-3_77.
[12] G. Tebaldi, E. Dave, A. Cannone Falchetto, M. Hugener, D. Perraton, A. Grilli, D. Lo Presti, M. Pasetto, A. Loizos, K.J. Jenkins, A. Apeagyei, J. Grenfell, M. Bocci, Recommendation of RILEM TC237-SIB on cohesion test of recycled asphalt, Mater. Struct. 51 (2018) 117, https://doi.org/10.1617/s11527-018-1238-4.
[13] S. Raschia, T.B. Moghaddam, D. Perraton, H. Baaj, A. Carter, A. Graziani, Effect of RAP Source on Compactability and Behavior of Cold-Recycled Mixtures in the Small Strain Domain, J. Mater. Civ. Eng. 33 (4) (2021) 04021030, https://doi.org/10.1061/(ASCE)MT.1943-5533.0003614.
[14] S. Raschia, A. Graziani, A. Carter, D. Perraton, Laboratory mechanical characterisation of cold recycled mixtures produced with different RAP sources, Road Mater. Pavement Des. 20 (sup1) (2019) S233–S246, https://doi.org/10.1080/14680629.2019.1588775.
[15] S. Raschia, A. Graziani, A. Carter, D. Perraton, Influence of RAP source and nominal maximum size on volumetric and physical properties of cement-bitumen treated materials, in: Transp. Res. Board 98th Annu. Meet., Washington DC, USA, 2019.
[16] S. Raschia, C. Mignini, A. Graziani, A. Carter, D. Perraton, M. Vaillancourt, Effect of gradation on volumetric and mechanical properties of cold recycled mixtures (CRM), Road Mater. Pavement Des. 20 (sup2) (2019) S740–S754, https://doi.org/10.1080/14680629.2019.1633754.
[17] P. Orosa, A.R. Pasandín, I. Pérez, Assessment of two laboratory design methods for CIR mixtures with bitumen emulsion based on static and gyratory compaction, Constr. Build. Mater. 265 (2020) 120667, https://doi.org/10.1016/j.conbuildmat.2020.120667.
[18] P. Orosa, A.R. Pasandín, I. Pérez, Compaction and volumetric analysis of cold in-place recycled asphalt mixtures prepared using gyratory, static, and impact procedures, Constr. Build. Mater. 296 (2021) 123620, https://doi.org/10.1016/j.conbuildmat.2021.123620.
[19] I. Pérez, B. Gómez-Meijide, A.R. Pasandín, A. García, G. Airey, Enhancement of curing properties of cold in-place recycling asphalt mixtures by induction heating, Int. J. Pavement Eng. 22 (3) (2021) 355–368, https://doi.org/10.1080/10298436.2019.1609674.
[20] M. Piratheepan, Designing Cold Mix Asphalt (CMA) and Cold-In-Place Recycling (CIR), Using SUPERPAVE Gyratory Compactor (2011).
[21] J.-C. Carret, A. Pedraza, H. Di Benedetto, C. Sauzéat, Comparison of the 3-dim linear viscoelastic behavior of asphalt mixes determined with tension-compression and dynamic tests, Constr. Build. Mater. 174 (2018) 529–536, https://doi.org/10.1016/j.conbuildmat.2018.04.156.
[22] J.-C. Carret, H. Di Benedetto, C. Sauzéat, Characterization of Asphalt Mixes Behaviour from Dynamic Tests and Comparison with Conventional Cyclic Tension-Compression Tests, Appl. Sci. 8 (2018) 2117, https://doi.org/10.3390/app8112117.
[23] A. Gudmarsson, N. Ryden, B. Birgisson, Characterizing the low strain complex modulus of asphalt concrete specimens through optimization of frequency response functions, J. Acoust. Soc. Am. 132 (4) (2012) 2304–2312, https://doi.org/10.1121/1.4747016.
[24] J.-C. Carret, H. Di Benedetto, C. Sauzéat, A. Tarantino, E. Ibraim, Dynamic testing of asphalt mixes, in, E3S Web Conf. 92 (2019) 04004, https://doi.org/10.1051/e3sconf/20199204004.
[25] D.L. Brown, R.J. Allemang, W.G. Halvorsen, Impulse technique for structural frequency response testing, J. Acoust. Soc. Am. 63 (S1) (1978) S81, https://doi.org/10.1121/1.2016847.
[26] J.-C. Carret, Linear viscoelastic characterization of bituminous mixtures from dynamic tests back analysis, University of Lyon, 2018.
[27] H. Di Benedetto, F. Olard, C. Sauzéat, B. Delaporte, Linear viscoelastic behaviour of bituminous materials: From binders to mixes, Road Mater. Pavement Des. 5 (sup1) (2004) 163–202, https://doi.org/10.1080/14680629.2004.9689992.
[28] F. Olard, H. Di Benedetto, General "2S2P1D" Model and Relation Between the Linear Viscoelastic Behaviours of Bituminous Binders and Mixes, Road Mater. Pavement Des. 4 (2) (2003) 185–224, https://doi.org/10.1080/14680629.2003.9689946.
[29] J.D. Ferry, Viscoelastic Properties of Polymers, 3rd ed., NY, USA, New York, 1980.
[30] S. Mangiafico, L.F.A.L. Babadopulos, C. Sauzéat, H. Di Benedetto, Nonlinearity of bituminous mixtures, Mech. Time-Dependent Mater. 22 (1) (2018) 29–49, https://doi.org/10.1007/s11043-017-9350-3.
[31] L. Babadopulos, G. Orozco, S. Mangiafico, C. Sauzéat, H. Di Benedetto, Influence of loading amplitude on viscoelastic properties of bitumen, mastic and bituminous mixtures, Road Mater. Pavement Des. 20 (sup2) (2019) S780–S796, https://doi.org/10.1080/14680629.2019.1628428.
[32] P. Orosa, I. Pérez, A.R. Pasandín, Evaluation of the shear and permanent deformation properties of cold in-place recycled mixtures with bitumen emulsion using triaxial tests, Constr. Build. Mater. 328 (2022) 127054, https://doi.org/10.1016/j.conbuildmat.2022.127054.
[33] S. Casillas, A. Braham, Quantifying effects of laboratory curing conditions on workability, compactability, and cohesion gain of cold in-place recycling, Road Mater. Pavement Des. 22 (10) (2021) 2329–2351, https://doi.org/10.1080/14680629.2020.1753101.